

Flow- and Diffusion Distributed Structures with noise at the inlet

Pavel V. Kuptsov^{a,*}, Razvan A. Satnoianu^b

^a*Department of Informatics, Saratov State Law Academy, Volskaya 1, Saratov
410056, Russia*

^b*Faculty of Actuarial Science, Cass Business School, City University, London
EC1Y 8TZ, UK*

Abstract

Flow and Diffusion Distributed Structures (FDS) are stationary spatially periodic patterns that can be observed in reaction-diffusion-advection systems. These structures arise when the flow rate exceeds a certain bifurcation point provided that concentrations of interacting species at the inlet differ from steady state values and the concentrations are held constant. Normally, theoretical studies of these patterns are developed without concerning a noise. In this paper we consider FDS for a more realistic conditions and assume that the inlet concentrations are perturbed by a small noise. When the flow rate is small, the FDS is linearly sensitive to noise at the inlet. Even weak fluctuations destroy the stationary pattern and an oscillatory solution appears instead. For higher flow rates the instability becomes nonlinear: the pattern remains unaltered for a weak noise and undergoes the destruction when the noise amplitude passes a certain threshold. We represent a detailed description of these effects and examine two scenarios for the stabilization.

Key words: Reaction-diffusion-advection system; Flow and Diffusion Distributed Structures; Flow Distributed Oscillations; Pattern formation; Noise

PACS: 82.40.Ck, 47.54.-r

1 Introduction

Reaction-diffusion system are known to demonstrate a variety of instabilities that result in stationary patterns or oscillatory behavior. Flow and Diffusion

* Corresponding author.

Email address: p.kuptsov@rambler.ru (Pavel V. Kuptsov).

Distributed Structure (FDS) is relatively new type of patterns that can appear in a reaction diffusion system in presence of an open flow. The necessary condition for this pattern to appear is oscillatory instability and constant, non steady state concentrations of interaction species at the inlet. If these condition are satisfied, the FDS appears when the flow rate passes above a certain critical point. Patterns of this type were first described by Kuznetsov et al. [1] and later they were studied in more details by Andresén et al. [2]. Soon after discovery these patterns were observed in the experiments by Kærn and Menzinger [3,4]. Later the experimental results were summarized in a survey paper [5].

There is a bit confusing variety of terms concerning this type of pattern formation phenomena. Initially, Kærn and Menzinger suggested the term “Flow distributed oscillations” (FDO) [3]. Later, the abbreviation FDS was suggested by Satnoianu [6,7]. In this paper we adhere to the last version and refer to the structures under consideration as FDS. (See also the discussion of the terminology in [8]).

Extensive theoretical studies of new structures are provided in [9,6,7,8]. In particular, these papers explore the relationship between FDS and other known types of instabilities in reaction-diffusion-advection systems: Turing patterns, DIFI and Hopf instabilities. As shown by McGraw and Menzinger in [8], the FDS (they use the term FDO, see the remark above) is closely related to the Hopf instability and DIFI, while the Turing pattern has a different nature.

As mentioned before, an FDS pattern emerges provided that a system demonstrates an oscillatory instability. Often a convective instability of the oscillatory mode is declared as a necessary condition for FDS: arbitrary small constant perturbation to the steady state at the inlet can grow to an FDS. But as shown by Kuptsov [10], the FDS can also appear in an absolute instability domain. In this case, however, the transition to FDS is rigid. If the inlet perturbation is small, the oscillatory solution dominates an FDS. However, the increasing of the perturbation gives an advantage to the FDS and it grows and suppresses the oscillations.

An experimental study of an FDS in presence of a differential transport is provided by Míguez et al. [11,12]. They consider a remarkable variety of impacts on an FDS pattern. These are a parallel formation of two neighboring FDSs, an FDS in a system with monotonically increasing flow rate, an FDS in 2D system with sinusoidally varying y -boundary and also interaction of two perpendicular FDSs. This analysis reveals a high degree of robustness and structural stability of this type of patterns.

A study of forcing to FDS is also presented in a work by Kuptsov et al. in [13]. This paper provides a numerical analysis of an FDS that is perturbed by a

small particle dragged by a flow. Papers [4,14,15] are devoted to the study of an FDS in presence of periodic oscillations at the inlet. We shall discuss these papers below in the final section, because they are closely related to our analysis.

Recently, Kuptsov et al. represented a theoretical analysis of FDSs in a 2D system with Poiseuille flow [16]. Two basic types of patterns were observed. The first one is y -dependant version of 1D FDS. The pattern consists of curved stationary stripes that are transverse to the flow direction. Patterns of this type were also observed in the experiments by Míguez et al. [12]. The second type of structures is specific to the 2D case: the structure consists of several stationary longitudinal stripes. If both types of basic structures are allowed, a more complicated pattern appears as a combination of transverse and longitudinal stripes.

All previous theoretical approaches have been developed for perfectly constant condition at the inlet. But fluctuations, that are always present in natural systems, can influence the pattern formation. As observed in many experiments, see for example [5] and [17], FDS near the critical point can be suppressed by oscillatory solutions induced by the inlet fluctuations.

The effect of an inlet noise on convectively unstable distributed systems was studied by many authors. We recall that in the convectively unstable system a growing perturbation drifts downflow but decays when observed from any fixed point. By contrast, absolute instability implies that the perturbation, being initially localized, grows at any fixed point in space [18,19,1,20] (see also reviews therein). In view of the extreme sensitivity of the convectively unstable state to perturbations, Deissler [21], Deissler and Farmer [22], and Borekmans et al. [23] conclude that wave-patterns may be generated and sustained due to amplification of fluctuations from an upstream noise source. More subtle than a straightforward amplification of noise, an interplay between fluctuations and dynamics is suggested by Landa [24] who treat the onset of turbulence in flow systems as a kind of noise-induced transition.

Kuznetsov [25] studied the effect of inlet noise on a spatially uniform reaction-diffusion-advection system. (This problem is similar to the ours, but we also apply a constant perturbation at the inlet to obtain an FDS pattern.) A noise-induced absolute instability was observed: the inlet noise increases the critical flow rate for transition from absolute to convective instability, and the new critical value is proportional to the square root of the noise amplitude, i.e., it obeys a power law.

In our previous paper [26] we already discussed the stability of FDSs to an inlet noise. In particular, we observed that when the flow rate is close to the FDS critical point, the noise, regardless of its amplitude, destroys the structure,

i.e., the FDS is linearly unstable. For higher flow rates the system passes a new critical point, thus becoming insensitive to a weak noise. Beyond this point, noise destroys the structure only when the noise amplitude exceeds a threshold value. The threshold grows as a power of the flow rate. We shall refer to this case as nonlinear instability of an FDS.

The purpose of the present paper is to extend our previous study. We demonstrate two scenarios of stabilization and develop a linear stability analysis of an FDS pattern. Sec. 2 reviews a variety of transitions to FDS. Sec. 3 represents a qualitative picture of the destruction and stabilization of FDSs by a noise. In Sec. 4 we summarize previous considerations and, employing Fourier analysis, introduce two scenarios of the stabilization. In Sec. 5 this two scenarios are confirmed by a linear stability analysis. Finally, Sec. 6 summarizes our results.

2 Oscillatory instabilities and transition to FDS

Before starting the main analysis let us introduce our model system and briefly review the oscillatory instabilities that can produce FDS patterns.

We shall consider the well-known Lengyel-Epstein model for the CIMA (chlorite-iodide-malonic acid-starch) reaction [27,28,6], assuming that the reagents are carried by a flow in a one-dimensional reactor:

$$u_t + \phi u_x - u_{xx} = a - u - 4uv / (1 + u^2), \quad (1a)$$

$$v_t + r\phi v_x - \delta v_{xx} = b \left(u - uv / (1 + u^2) \right). \quad (1b)$$

Here u and v denote the dynamical variables related to the concentrations of two chemical species, a and b are treated as control parameters, and ϕ is the flow rate. The transport rates for u and v can be different: δ introduces the differential diffusion, and r controls the differential flow. We shall study two cases: no differential flow at $r = 1$ and identical ratios for diffusion and flow at $r = \delta$. The reactor is supposed to be semi-infinite.

Note that we use a nonstandard form of Eqs (1). Normally, in the model equations for CIMA reaction parameters δ and b are proportional to each other. But in all our studies we always take *a constant* values for the parameters and analyze the varying of the flow rate or noise amplitude. So, at each step of observations one can easily recalculate our parameters to the standard ones. But we believe that the specific numerical values are not very important because we do not study the system near bifurcation points. As we have examined, the represented results remain valid for a wide variety of the parameter values.

We shall find numerical solutions to Eqs. (1) via the semi-implicit Crank-Nicholson method with steps of discretization $\Delta x \approx 0.1$ and $\Delta t \approx 0.0125$. Also, in all our numerical simulations an outlet condition $(u_x, v_x)_{x=X} = 0$ is applied, where X is the length of the reactor. This type of the outlet conditions are normally used in numerical simulations of reaction-diffusion systems, see for example [28,1]. These conditions are the best choice for a model of a semi-infinite, i.e., very long, system. In such a system the right boundary should not influence an overall picture. The vanish of u_x and v_x at the outlet effectively prevents an upstream propagation of any numerical artifacts. They, if appear at all, stay near the right boundary as a tiny area of oscillations.

The system (1) admits the homogeneous steady state solution

$$u_S = a/5, \quad v_S = 1 + a^2/5^2. \quad (2)$$

In the absence of a flow the steady state can be destabilized either by Hopf or by Turing modes whose growth rates becomes positive at

$$b = b_H = (3a^2 - 125)/(5a) \quad (3)$$

and

$$b = b_T = (125 + 13a^2 - 4a\sqrt{10(25 + a^2)})\delta/(5a), \quad (4)$$

respectively [29,30,28]. The Hopf instability gives rise to uniform temporal oscillations while the Turing instability produces a stationary space-periodic pattern. Note that for the considered system supercritical values of b lie below the bifurcation points.

When both components of the system are transported by a flow with identical rates, i.e., $r = 1$, the Hopf instability remains unaltered while the Turing structure loses its stationarity. (Of course, this takes place only for an observer in a laboratory reference frame. The other one that moves with the flow still registers normal Turing stripes). The frequency of temporal oscillations of the appearing waves is proportional to the flow rate [31].

Differential flow with $r \neq 1$ results in the formation of new spatio-temporal structures due to the so-called Differential-Flow Instability (DIFI) [32]. The most interesting situation is observed outside the Hopf and Turing domains. The homogeneous steady state of the system remains stable until the flow rate reaches a critical point ϕ_{DIFI} . Above this point, a DIFI mode become unstable and give rise to travelling waves.

In presence of a flow an instability can be either absolute or convective. The absolute instability appears for small flow rates and manifests itself as a spreading of an initially localized perturbation over the whole space. For higher flow rates the instability becomes convective: the growing perturbation, being carried by the flow, decays in any fixed point. A critical point ϕ_{ca} for the transition from

absolute to convective instability can be obtained from dispersion equation of a system as described in [18,19,1,20] (see also reviews therein).

Figure 1 represents solutions to Eqs. (1) that are induced by the instabilities described above. In the other words, this figure demonstrates what happens in our system without an FDS. For all panes of the figure the initial condition at $t = 0$ is the homogeneous steady state perturbed by small, spatially inhomogeneous fluctuations. The inlet is held at the steady state.

Figure 1(a) illustrates a convective Hopf instability. We observe a temporally periodic structure with a wave number that is zero on average. Because the initial distribution of the reacting species is inhomogeneous, Hopf oscillations appears in different points with different initial phases. Zero wave number of a Hopf mode means that the effective interaction between neighboring points is very weak. As a result we observe in the figure a lot of local phase perturbations. The perturbations, however, are slowly smoothed out by the diffusion. These perturbations as well as the upstream edge of the structure travel down-flow. This confirms the convective nature of the observed instability. Note that this is dictated by a dispersion equation and does not depend on boundary or initial conditions. One can easily reproduce this convective moving of the spatio-temporal structure for different conditions at the system edges or for another inial perturbation.

Figure 1(b) represents a spatio-temporal structure that appears due to an absolute Turing instability. The initial state for this figure is inhomogeneous, but, in contrast to the Hopf case, the structure forms due to the spatial interaction stimulated by a differential diffusion. This process subordinates the concentrations of the reacting species in different points and results in the perfect spatially periodic pattern. In a spatio-temporal diagram this should looks like a vertical stripes. But a flow transports the Turing structure. As a result we observe that the stripes are sloped exactly along the flow. (In the spatio-temporal diagram $\phi = 0.5$, $t_{\max} = 200$ and $x_{\max} = \phi t_{\max} = 100$, so that the flow is parallel to the main diagonal).

Finally, Fig. 1(c) illustrates a DIFI structure. For the parameters values that are used for this figure, the system is stable without a flow, but different flow rates of the reactants produces an instability. Now both frequency and wave number are nonzero. Observe that they have opposite signs, and DIFI waves travel upstream. The DIFI takes place at ϕ_{DIFI} that is normally higher than the critical value for absolute-convective instability transition ϕ_{ca} . In our case the DIFI is also convective, so that the structure is washed by a flow.

FDS patterns appear in the system when temporal oscillations are spread in space by a flow. Every volume of an oscillating medium, being carried by the flow, appears with different phases in different spatial points and thereby pro-

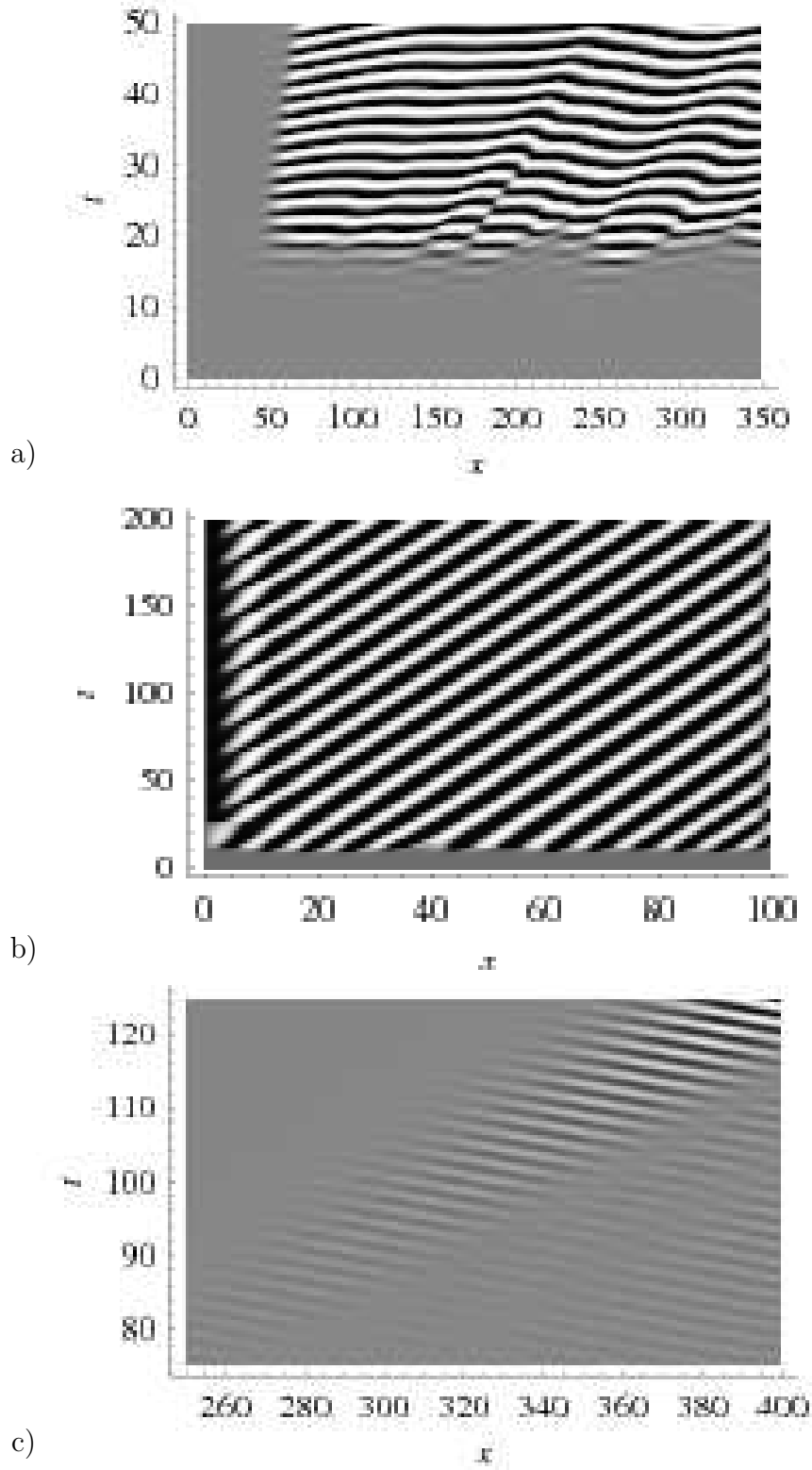


Figure 1. Oscillatory instabilities in the system (1). Grey levels indicate values of u . For all panels $a = 20$. (a) Hopf instability at $b = 6$, $\delta = 3$, $r = 1$, $\phi = 3$. (b) Turing instability at $b = 6$, $\delta = 15$, $r = 1$, $\phi = 0.5$. (c) DIFI at $b = 12$, $\delta = r = 3$, $\phi = 1.5$.

duces a spatially periodic structure. The flow rate is constant, so this structure is stationary if all portions have identical initial phases. For this to be fulfilled, a constant boundary perturbation should be applied at the inlet. This is a permanent displacement of reagent concentrations from the homogeneous steady state. A wave number of FDS can be roughly estimated as ω/ϕ , where ω is the frequency of the oscillations registered in a reference frame that moves with the flow (see discussion in [2,3,33,34]).

A Hopf mode is responsible for the formation of FDS when all components of the system have identical flow rates. In the presence of a differential flow this role is played by a DIFI mode. Turing oscillations can not produce an FDS because this solution is stationary in the co-moving reference frame, so that for a stationary observer every portion of a medium moves along the system with constant phase. This simple conclusion is in a good agreement with the analysis provided by McGraw and Menzinger [8]: the FDO/FDS patterns are shown to be closely related to Hopf instability and DIFI, while the Turing pattern formation mechanism has a quite different nature.

To realize the formation of FDS, it is enough to perturb only one of the components and keep steady state value for the other:

$$u(x = 0, t) = u_S + u_{\text{bnd}}, \quad v(x = 0, t) = v_S, \quad (5)$$

where u_{bnd} is a constant perturbation of the boundary value. As before, u_S and v_S represent the homogeneous steady state. When the flow rate is small, the perturbation decays in space. A non-decaying FDS solution appears above a critical point [1,2,6],

$$\phi_{\text{FDS}} = \sqrt{\frac{40a^3b(\delta + r)^2 - (3a^2\delta + 5ab - 125\delta)^2r}{(25 + a^2)(\delta + r)(3a^2r - 5ab - 125r)r}}. \quad (6)$$

This critical value diverges at $b = rb_H$. Without a differential flow, i.e., at $r = 1$, the condition of divergence coincides with the condition for the Hopf instability, while at $r > 1$ an FDS appears even if the flow-less system is stable.

If $\phi > \phi_{\text{FDS}}$ and $\phi > \phi_{\text{ca}}$, the transition to FDS takes place when an oscillatory mode is convectively unstable. Because in this case growing oscillations travel with the flow, any small inlet perturbation can freely grow to the FDS pattern. This case is referred to as a soft transition to FDS [20,10]. Otherwise, if $\phi_{\text{FDS}} < \phi < \phi_{\text{ca}}$, the oscillatory mode is absolutely unstable and tends to occupy the whole space. Now the FDS can grow only when the inlet perturbation is high, because it must overcome the competition from the oscillatory solution. This is a rigid transition to FDS [20,10]. In this paper we analyze FDS for $\phi > \phi_{\text{ca}}$, i.e., we are interested in the case of the soft transition.

3 FDS in presence of inlet noise: a qualitative picture

We introduce a noise via the following boundary condition at the inlet:

$$u(x = 0, t) = u_S + u_{\text{bnd}}(1 + \theta \xi(t)), \quad v(x = 0, t) = v_S. \quad (7)$$

Here, u_S and v_S denote the homogeneous steady state and u_{bnd} is the constant boundary perturbation. $\xi(t)$ describes a noise with the uniform distribution in the interval $[-1, 1]$, and θ controls an amplitude of the noise relating to u_{bnd} . The particular distribution of a noise is not very important. But, as we explain below, it should be sufficiently wide to contain required harmonics.

In our previous work [26] we have studied the stability of FDS patterns in the Hopf oscillatory domain. In this paper we consider the following four cases.

- (1) FDS appears in presence of the Hopf instability: $r = 1$ and $b_T < b < b_H$.
- (2) FDS is observed in presence of a differential flow, $r > 1$. The system is stable without a flow, i.e., $b > b_H$ and $b > b_T$. Oscillations appear due to DIFI when the flow rate is above a critical point ϕ_{DIFI} .
- (3) The transition to FDS takes place when both Turing and Hopf modes are unstable: $r = 1$ and $b \ll b_H < b_T$. The Turing mode has a higher growth rate, but the Hopf mode is also significant.
- (4) FDS appears again in the presence of Hopf and Turing modes, but the system is close to the Hopf point: $b \lesssim b_H$. Growth rate of the Hopf mode is small, so that this mode is much weaker than the Turing one.

The analysis developed in [26] shows that in presence of an inlet noise the FDS is destroyed at small flow rates and appears only when the flow rate passes a certain point of stabilization. The stabilization flow rate is found to depend on the noise amplitude as a power law. For a fixed flow rate the FDS is stable if the noise amplitude is small and the pattern is destabilized and destroyed when the amplitude passes a certain threshold. In the present paper we refer to this phenomenon as a nonlinear instability of FDS. The picture differs for flow rates a bit above the FDS critical point ϕ_{FDS} . The threshold noise level is absent and FDSs are linearly unstable so that any small inlet fluctuations destroy the pattern. We already reported this case in [26]. In Sec. 5 a detailed investigation is provided.

3.1 Case 1: Hopf instability

Figure 2 demonstrates an interaction between an FDS and inlet noise when only a Hopf mode is unstable. The constant part of the inlet perturbation is small, so that the FDS in this figure has a boundary layer. A structure

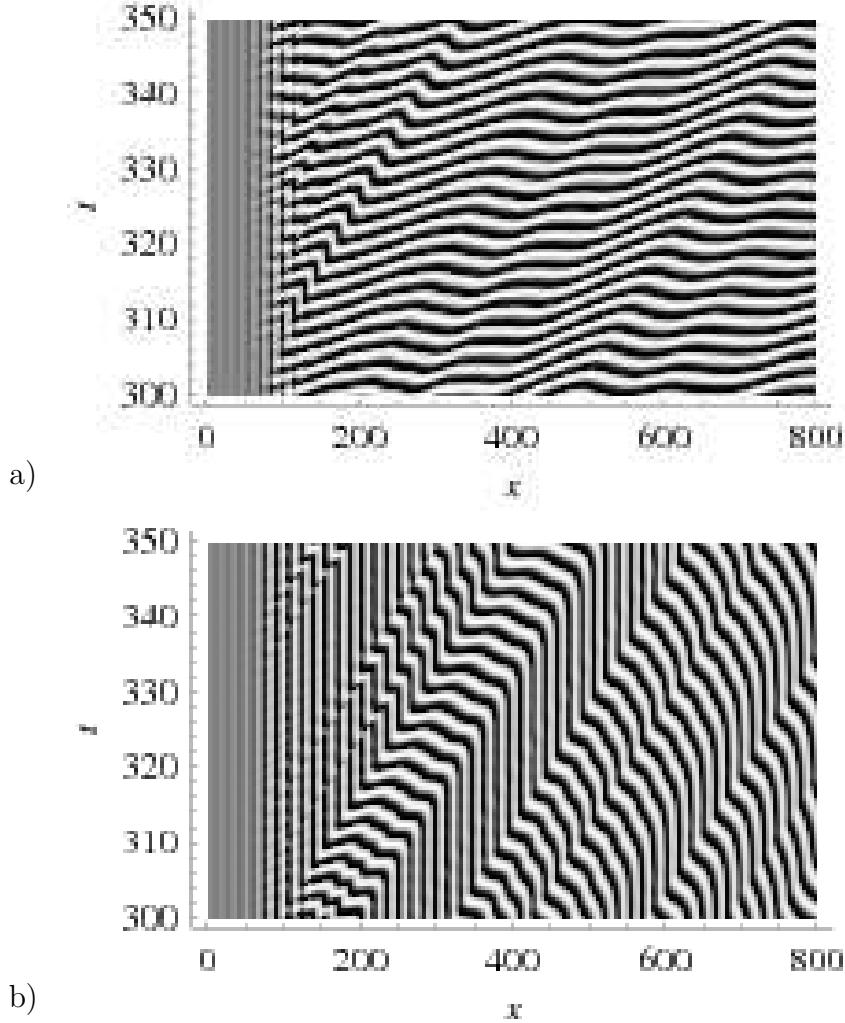


Figure 2. FDS in the presence of inlet noise when a Hopf mode is unstable. In panel (a) the noise destroys the FDS pattern, while in panel (c) (see below) the FDS is stabilized at a higher flow rate. Flow rate grows from (a) $\phi = 6$ to (b) $\phi = 6.5$ and (c) $\phi = 7$. $a = 20$, $b = 6$, $\delta = 3$, $r = 1$, $u_{\text{bnd}} = 0.1$, $\theta = 0.05$ ($b_{\text{H}} = 10.75$, $b_{\text{T}} \approx 3.289$).

without a boundary layer is stabilized at smaller flow rate and has a number of peculiarities that we shall discuss below.

In Fig. 2(a) the FDS pattern disappears after several periods and a new oscillatory structure forms instead. This effect can be explained by a selective amplification of Fourier components of the noise. The maximum of this amplification corresponds to a Hopf mode [26]. This results in a resonant excitation of this mode by the noise so that a growing oscillatory solution destroys the FDS. A corresponding Hopf structure without a noise is shown in Fig. 1(a). Note a high degree of similarity between noise and noiseless solutions.

If an FDS has a boundary layer, i.e., u_{bnd} is small, the amplification basically

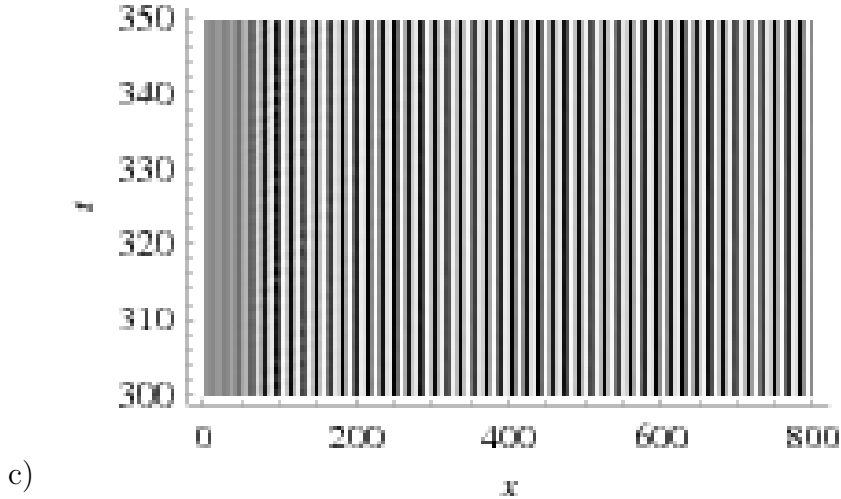


Figure 2. (*continued*)

occurs inside this layer. A perturbation to the pattern always manifests itself at the end of the boundary layer regardless of the flow rate, compare Figs. 2(a) and (b). If u_{bnd} is high and the boundary layer is absent, the noise also destroys an FDS pattern. But an effective amplification ratio of a fully developed FDS pattern is much lower, so that the length of an unperturbed FDS area can be very long. (We do not provide an illustration because, except for the boundary layer, the spatio-temporal diagram looks as that in Fig. 2(a)).

Figure 2(b) illustrates an intermediate situation for a higher flow rate. Now the influence of the noise is weaker and the FDS is not totally destroyed. The overall structure is a composition of vertical fragments of FDS and sloped stripes of an oscillatory solution. Observe a remarkable regularity of this composition. This interesting structure appears because both the stationary stripes and the oscillatory fragments are different manifestations of a Hopf solution. (Recall that FDS is, in fact, an oscillations that are spread in space due to a flow and diffusion.) This explains why the fragment are joined so well into continuous step-like stripes.

This type of structures is a typical response of an FDS to a perturbation. Kærn and Menzinger [4] first observed them in a system with oscillatory inlet boundary [4]. The structures was referred to as pulsating waves. A more complicated zigzag patterns are reported by Taylor et al. [17]. Also, similar structures was described by Kuptsov et al. [13] for an FDS perturbed by a moving particle. In addition, coexisting stationary and travelling waves have been observed in a system without noise [7].

FDS without a boundary layer can also demonstrate spatio-temporal structures composed of stationary and oscillatory fragments. An example is shown in Fig. 3. As mentioned above, for FDS without a boundary layer the ampli-

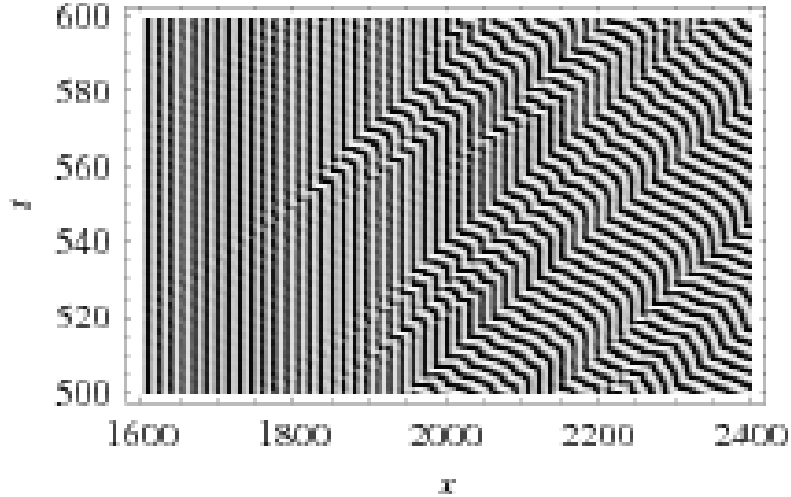


Figure 3. Spatio-temporal intermittency for an FDS without a boundary layer. The parameters are as in Fig. 2 except $\phi = 6.1$ and $u_{\text{bnd}} = 2$. Unlike Fig. 2(b), the structure appears far from the inlet.

fication area can be very extended. In Fig. 3 the FDS at $x < 1800$ looks like a noiseless pattern. However, beyond this point noise demonstrates itself. Note that the flow rate in Fig. 3 is less than in Fig. 2(b). In other words, an FDS without a boundary layer is less sensitive to noise and becomes stable at a smaller value of the flow rate.

Further increase of the flow rate results in the growth of the stationary fragments and shrinking of the oscillating ones. Finally, all oscillating fragments disappear and we observe a pattern as in Fig. 2(c). The structure here looks like a perfect FDS without a noise.

Figure 4 provides a more accurate verification of the stabilization. This figure shows spatial distributions of variances of temporal oscillations. The distributions are calculated for the diagrams in Fig. 2. Labels (a), (b) and (c) on the curves correspond to the panels of Fig. 2. All curves grow exponentially within the boundary layer of the FDS and nearly coincide there. In other words, the boundary layer amplifies noise even when the corresponding fully developed FDS is stable. Behind the boundary layer the curves behave differently. Curve (a) continues to grow and reaches a saturation very fast. This corresponds to the oscillations observed in the right part of Fig. 2(a). The intermediate curve (b) also grows, but does not tend to saturation. It varies slowly and irregularly near a relatively high value. This occurs because time series in this case are composed of fragments of two solutions, see Fig. 2(b). They are irregularly arranged and their sizes are distributed within a wide range. Curve (c) confirms the stabilization. The variance decays, therefore, the FDS remains stable even far downflow.

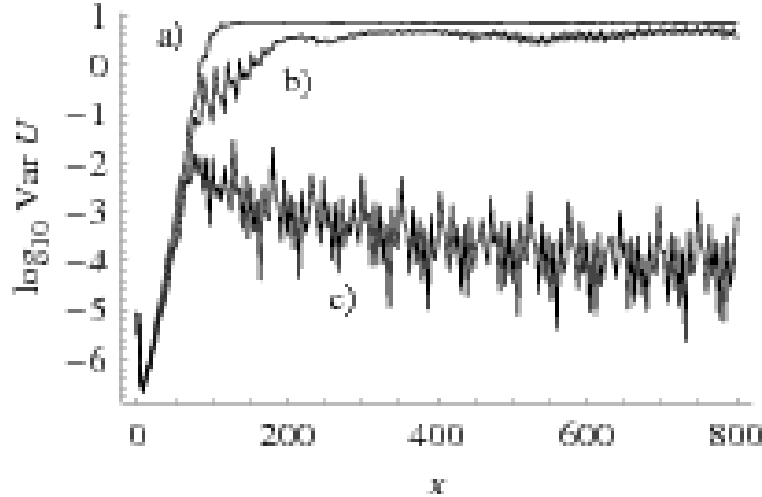


Figure 4. Spatial distributions of the variances of temporal oscillations before, curves (a) and (b), and after the stabilization of FDS, curve (c). The curves correspond to the panels in Fig. 2 with respective letters.

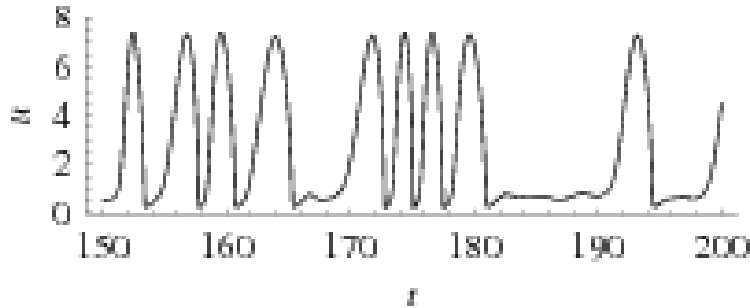


Figure 5. Intermittent time series of u recorded in a fixed spatial point for the case represented in Fig. 2(b). Laminar phases correspond to fragments of FDS stripes.

The combination of stationary and oscillatory solutions that is demonstrated in Figs. 2(b) and 3 can be treated as a spatio-temporal intermittency. A similar compound structure has been analyzed by Kuptsov et al. [13]. Figure 5 demonstrates an example of an intermittent time series. Variable of u is observed from a fixed point in space: laminar phases, that correspond to fragments of FDS, are interrupted by bursts of oscillations.

A characteristic feature of intermittency is a power-law divergence of the mean length of laminar phases as a bifurcation parameter approaches a critical point. In our case the flow rate controls the mean length of FDS fragments and the divergence corresponds to the stabilization of FDS. Let us employ the following algorithm: Given the flow rate, we compute a pure FDS pattern without a noise. Then we take a point at some distance from the inlet where the FDS is definitely fully developed (for all computations we take the same point). Starting from this position, within the period of the FDS we seek another

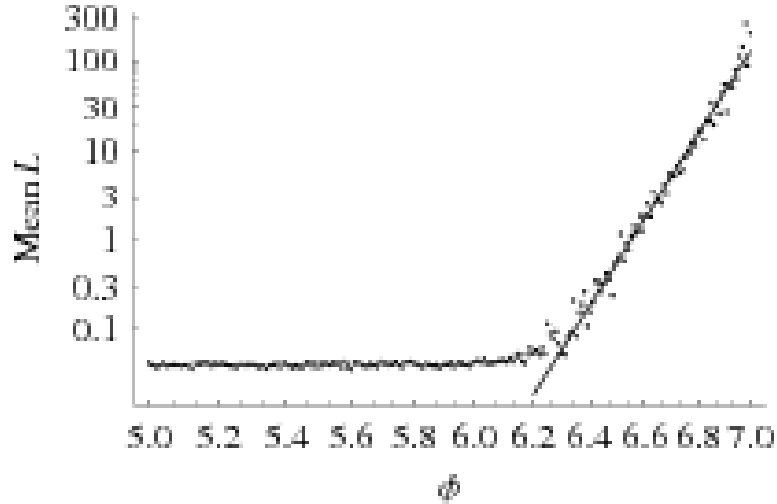


Figure 6. Mean lengths of FDS fragments vs. flow rate measured in a fixed spatial point. The parameters are as in Fig. 2. The dots, computed numerically, are plotted in double logarithmic scale. In the right part the numerical data are approximated well by a straight line that indicates a power-law dependence. The exponent, equal to the slope of the line, is $\gamma \approx 73$.

point where u is in the middle between its maximum and minimum values. The value of u in this point is treated as a laminar state. Now a noise is switched on and after a transient period the mean time of staying near the laminar state is registered. Repeating this procedure for different flow rates, we obtain the dependence shown in Fig. 6. When the flow rate is small, u oscillates, as shown in Fig. 2(a), and passes the laminar state very fast. In Fig. 6 the corresponding mean values are very small. Intermittency appears for $\phi > 6.2$, and the mean time spent near the laminar state starts to grow with the flow rate. The numerical data in this part of the figure are approximated well by a straight line in double logarithmic scale. This implies a power-law dependence $\langle L \rangle = (\phi - \phi_c)^\gamma$. Note that the exponent $\gamma \approx 73$ is extremely high.

3.2 Case 2: DIFI

This case, illustrated in Fig. 7, is similar to the previous one. In Fig. 7(a) we observe how a noise excites an unstable oscillatory mode that grows to an oscillatory solution. But now a DIFI mode is responsible for the formation of FDS. Hence, it is the DIFI solution that appears behind the destructed FDS. Observe the high regularity of the appearing structure. In Fig. 7(b) a higher flow rate results in the formation of spatio-temporal intermittency similar to the structure in Fig. 2(b). A perfect correspondence between stationary and oscillatory fragments is also observed. The explanation is as in the previous

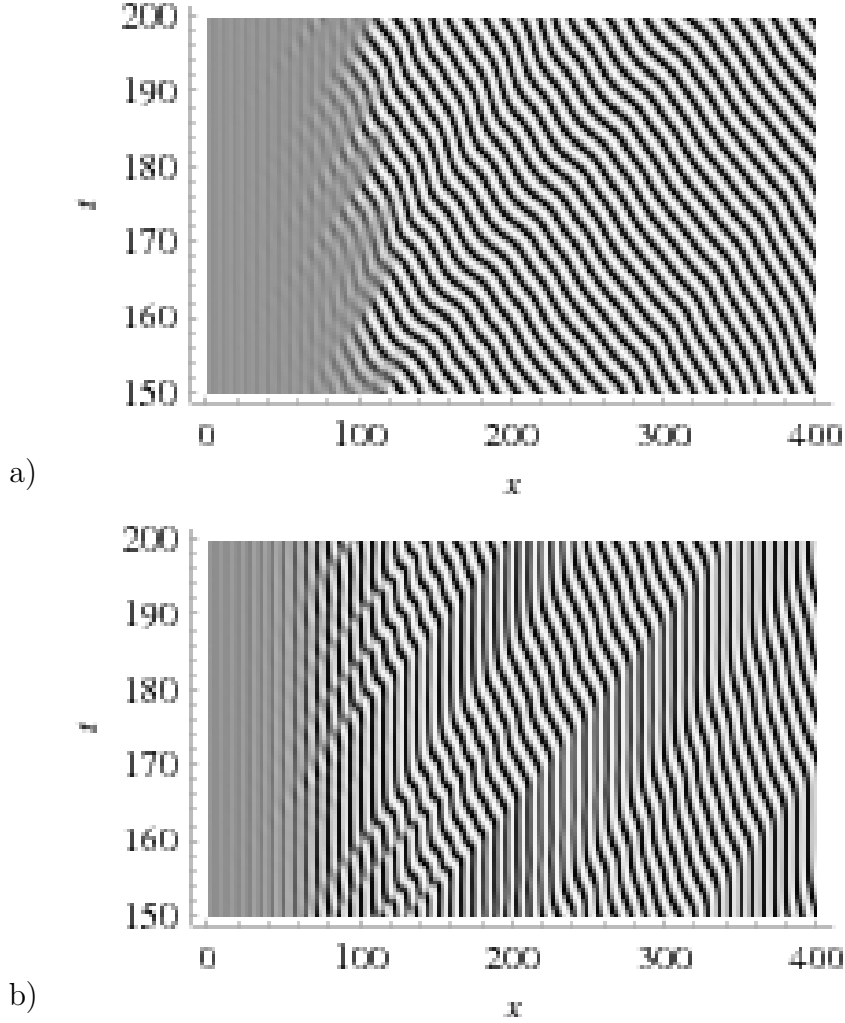


Figure 7. FDS with noise when a DIFI mode is unstable: (a) $\phi = 2.3$, and (b) $\phi = 2.47$. $a = 20$, $b = 12$, $\delta = r = 3$, $u_{\text{bnd}} = 0.1$, $\theta = 1$ ($b_{\text{H}} = 10.75$, $b_{\text{T}} \approx 3.289$, $\phi_{\text{DIFI}} \approx 1.47$ and $\phi_{\text{FDS}} \approx 2.27$).

case: On the one hand, the DIFI mode produces the oscillatory solution and, on the other hand, it is responsible for the formation of FDS. Further increase of the flow rate results in the stabilization of the FDS. Note that the noise amplitude is very high: $\theta = 1$. This is even higher than the constant part $u_{\text{bnd}} = 0.1$ of the inlet perturbation. But this can not prevent the stabilization. The pattern looks as in Fig. 2(c) and is not shown here.

As one can see from Fig. 7, the boundary layer of the FDS manifests itself in a similar way as in the case shown in Fig. 4. The boundary layer effectively amplifies the noise, so that the oscillatory solution appears near its right edge. A structure without a boundary layer can also amplify noise, but the area of amplification is very extended and grows when the flow rate becomes higher. In particular, one can observe spatio-temporal intermittency only far from the

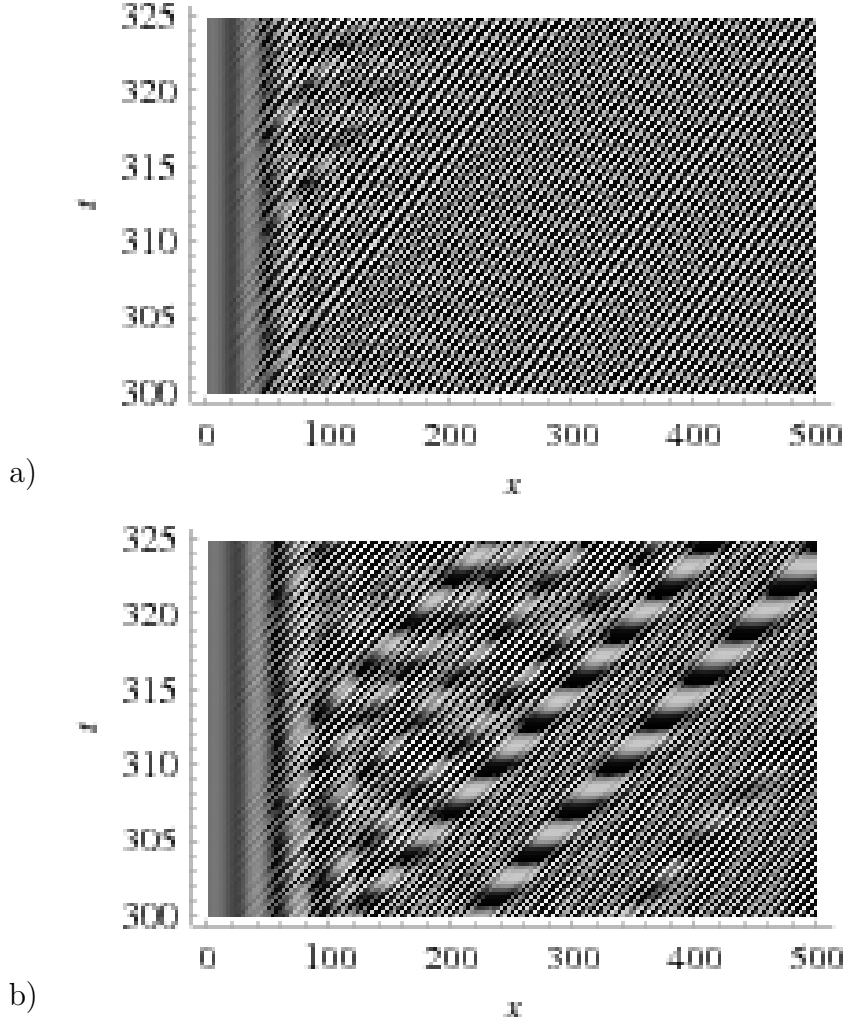


Figure 8. FDS with noise in the presence of Turing and Hopf modes with significant growth rates. For all panels $a = 20$, $b = 5$, $\delta = 20$, $r = 1$, $u_{\text{bnd}} = 0.5$, $\theta = 0.1$ ($b_{\text{H}} = 10.75$, $b_{\text{T}} \approx 21.928$). Panels correspond to different flow rates: a) $\phi = 10$, b) $\phi = 12$.

inlet. As in the previous case, FDS without a boundary layer is stabilized at a smaller flow rate in comparison to the structure that has a boundary layer. The described behavior of FDS with and without a boundary layer is typical. We have also analyzed the effect of boundary layers for the two remaining cases and obtained similar results.

3.3 Case 3: Turing and Hopf modes with significant growth rates

Now we assume that $b \ll b_{\text{H}} < b_{\text{T}}$, so the system displays both Hopf and Turing significant unstable modes and the Turing mode has a higher growth rate. As follows from direct numerical simulations, in a corresponding unbounded

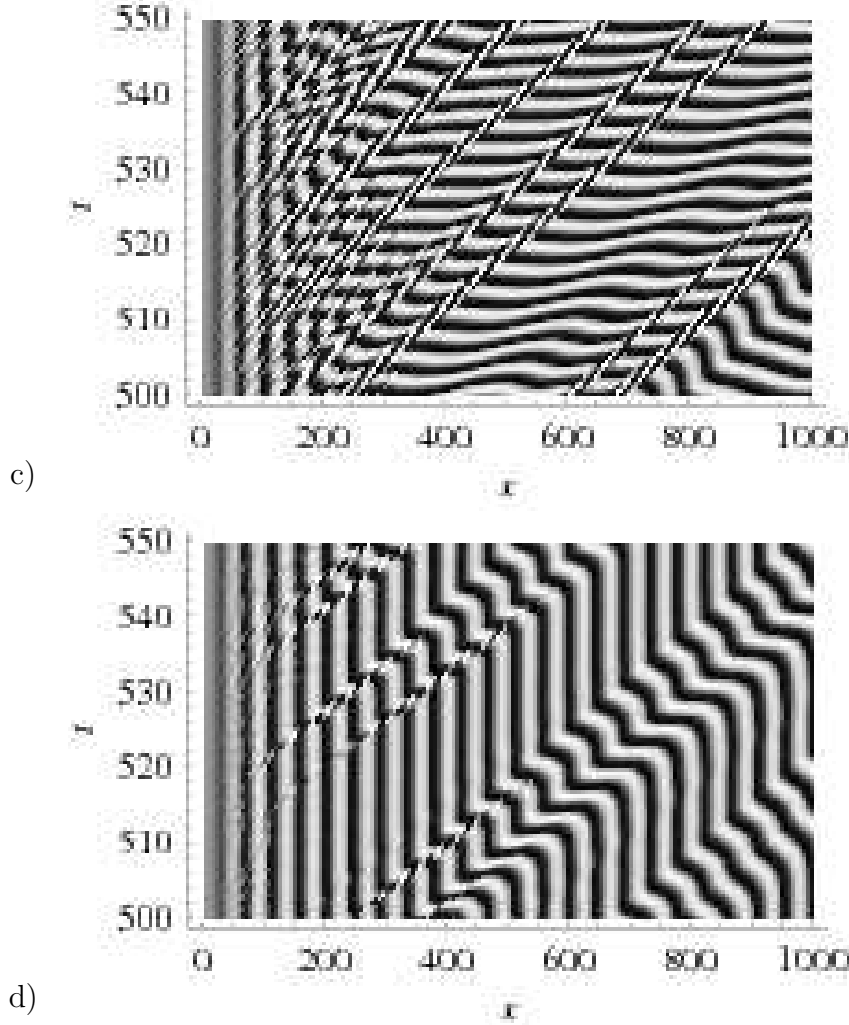


Figure 8. (*continued*) The flow rates in the panels are c) $\phi = 14$, d) $\phi = 15.5$.

noiseless system the Turing solution grows faster and suppresses the Hopf one.

Let us begin from small flow rates. When the FDS is affected by a noise, the Turing mode suppresses both the FDS and Hopf solutions and we observe almost perfect Turing structure behind a narrow FDS area, see Fig 8(a). This figure is qualitatively similar to Figs. 2(a) and 7(a) where unstable oscillatory modes also grow to form spatio-temporal structures in place of a destroyed FDS.

Contrary to the previous cases, the higher flow rate in Fig. 8(b) does not result in the reestablishment of FDS. It gives an advantage to the Hopf mode instead. This one manifests itself as localized travelling areas of oscillations embedded into the Turing structure.

Further increase of the flow rate makes the Hopf mode stronger, see Fig. 8(c). The Turing waves appear now as localized perturbations to the Hopf structure.

In the other words, we have another spatio-temporal structure produced by the strongest oscillatory mode that suppresses the FDS.

If the flow rate continues to grow, the Hopf solution starts to give up its area to the FDS. This produces a spatio-temporal intermittency, Fig. 8(d). Note that a Turing structures disappear in a different manner. In this figure there are rare localized Turing waves that are swept by the flow and decay in space. Sufficiently far from the inlet a combination of oscillatory and stationary solutions appears in the same manner as in the previous cases, see Figs. 2(b) and 7(b). As the flow rate increases even further a stabilization of the FDS takes place. We do not provide a corresponding figure because the pattern looks like in Fig. 2(c).

3.4 Case 4: Turing instability in presence of a weak Hopf mode

This case differs from three previous. Though a Hopf mode is unstable and give rise to the formation of FDS, there is another unstable mode, namely the Turing one, that has much higher growth rate. When the flow rate is small, the spatio-temporal structure is as in the previous case. Figure 9(a) shows how a noise stimulates the growth of a Turing solution in place of the FDS while the Hopf mode does not manifest itself at all (compare with Fig. 8(a)). But now even when the flow rate becomes higher a Hopf solution does not emerge. The left end of the Turing area becomes indented, and we observe an intermittent structure, Fig. 9(b). Unlike three previous structures, oscillatory and stationary fragments here have different origins. The stationary FDS stripes appear due to the Hopf mode while the oscillatory segments are produced by the Turing mode. Hence, fragments of different solutions are not joined into continuous, smooth zig-zag structures. They overlap and partially suppress each other instead. When the flow rate continues to grow, the FDS segments are enlarged while the Turing areas becomes more and more rare. Finally, the FDS becomes stable and occupies the whole space. The resulting pattern looks like in Fig. 2(c).

4 Two scenarios of stabilization

Four cases considered above demonstrate two different scenarios of stabilization. The first one involves cases 1, 2 and 3, while the second is represented by the case 4. A clearer evidence of this can be provided with the Fourier analysis: We are going to demonstrate the dependance of Fourier spectra of time oscillations on the flow rate. This can be done with the following procedure. A point is fixed near the outlet and a series of temporal oscillations is

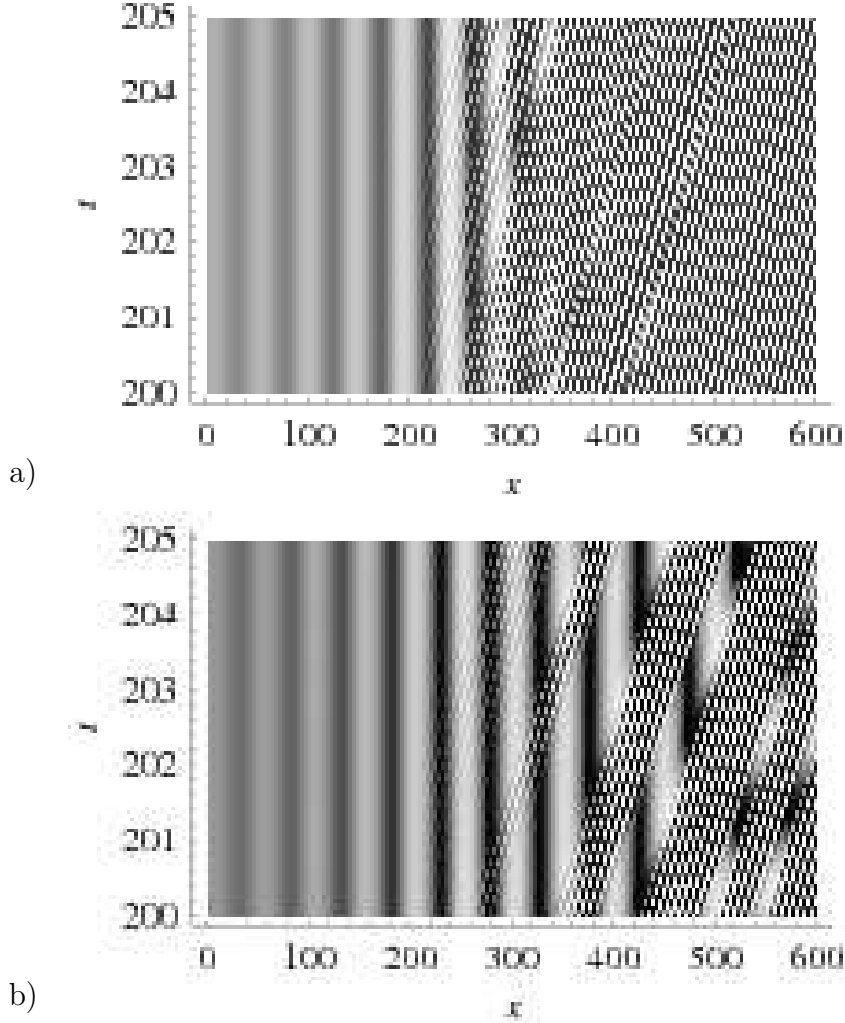


Figure 9. FDS with noise when a Turing mode is strong while a Hopf mode is weak. Observe the formation of Turing structure in place of the FDS in panel (a), $\phi = 22$, and spatio-temporal intermittency in panel (b), $\phi = 23.5$. The parameters are $a = 25$, $b = 10$ ($b_H = 14$, $b_T = 37.549$), $\delta = 25$, $r = 1$, $u_{\text{bnd}} = 0.5$, $\theta = 10^{-5}$.

recorded in this point. Then the mean value of the series is subtracted and Fourier spectrum is computed using the FFT algorithm. This is repeated for different flow rates and the resulting Fourier amplitudes are plotted via grey scales in Fig. 10. The panels (a), (b), (c) and (d) in this figure correspond to Figs. 2, 7, 8 and 9, respectively.

As we already discussed in our previous paper [26], the destruction of FDS takes place because this pattern can selectively amplify a noise and the peak amplification corresponds to the unstable oscillatory mode. This is confirmed in Fig. 10. We see here that Fourier components are gathered around an unstable modes of the system. The resonant interaction between selected harmonics and internal unstable modes results in the destruction of FDS.

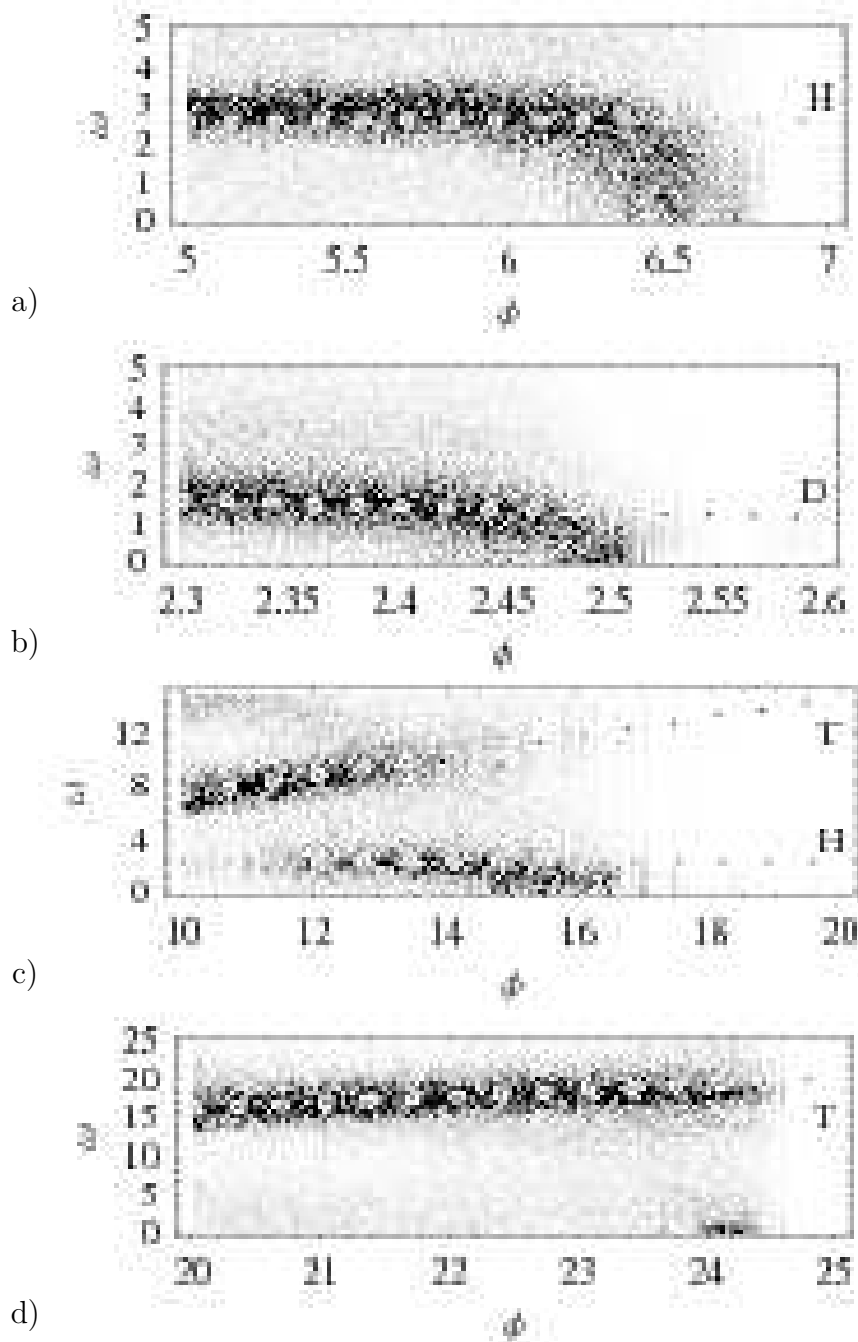


Figure 10. Fourier spectra of temporal oscillations vs. flow rate at a fixed point near the outlet. Grey levels indicate values of Fourier amplitudes. Panels (a), (b), (c) and (d) (see below) correspond to Figs. 2, 7, 8 and 9, respectively. Dashed lines show Hopf (H), Turing (T) and DIFI (D) frequencies. Light areas on the right parts of the figures correspond to the stable FDS.

Figures 10(a) and 10(b) demonstrate that the stabilization in the Hopf and DIFI cases occurs due to the detuning of the selected harmonics from the resonance. Bands of selected frequencies are shifted down. Though the noise is still amplified, but the selected frequencies differ from the resonant and, hence, can not produce intensive excitation of the oscillations. The amplitudes of the outlet oscillations are reduced. We observe in the figure that the shaded areas becomes lighter as the flow rate grows. This corresponds to an intermittency in the spatio-temporal diagrams, see Figs. 2(b) and 7(b). The shift of the frequencies is reflected in these figures by the partial straightening of the oscillatory segments that occur due to the merging with vertical FDS stripes (compare, for example, the Hopf structure in Fig. 2(a) and the oscillatory areas in Fig. 2(b)).

Figure 10(c) illustrates the same scenario of the stabilization. This takes place via the detuning of selected frequencies from the resonance with the Hopf mode. But here another band of Fourier components appears around the Turing mode. When the flow rate is small, noise is not amplified near the weak Hopf mode. The resonance with the Turing mode is responsible for the formation of the oscillatory solution in Fig. 8(a). For a higher flow rate both modes are excited by the noise harmonics and we observe a spatio-temporal structure as in Fig. 8(b). Unlike the Hopf mode, the selective amplification around the Turing frequency does not depend directly on the flow rate and the Fourier components remain gathered around the Turing mode. But the coefficient of amplification vanishes as the flow rate grows: the shaded area in the figure becomes lighter. The corresponding spatio-temporal structure is shown in Fig. 8(c). Finally, the Turing band disappears and further stabilization proceeds as in previous panels (a) and (b) of Fig. 10. The corresponding spatio-temporal diagram in Fig. 8(d) is also similar to the Hopf and DIFI cases, Figs. 2(b) and 7(b), respectively.

Fig. 10(d) illustrates the second scenario of the stabilization. The selective amplification takes place only around the Turing mode, while the Hopf mode does not manifest itself except the small area at $\phi \approx 24$. The gathering of the Fourier components near the Turing mode is similar to the case 3, see Fig. 10(c). But now this is the main mechanism responsible for the stabilization. Observe that the shaded area in Fig. 10(d) disappears very sharply. This is explained by an intermittent nature of analyzed time series, see Fig. 9(b). When the flow rate approaches the stabilization point, intervals between Turing bursts grow and sooner or later we get an interval that is longer than the observation time. In this point the characteristic Fourier spectrum suddenly disappears. Though in the previous case 3 the Turing oscillations also demonstrate a kind of intermittency with the Hopf solution, see Fig. 8(b), the corresponding Fourier components in Fig. 10(c) disappear smoothly. It indicates that there the intervals between Turing areas do not diverge.

5 Linear stability analysis

In our previous paper [26] we have found that near the critical point ϕ_{FDS} an FDS pattern is linearly unstable and any small perturbation applied at the inlet can destroy it. In this section we study this effect and develop a linear stability analysis of the FDS.

Let us first recall the discussions of Fig. 4. This figure displays spatial distributions of the variances of temporal oscillations of u . The variances, both before and after the stabilization point, grow exponentially within the boundary layer of FDS. The stabilization reveals itself only for a fully developed FDS while the boundary layer always amplifies noise. We have observed this for many parameter values and believe that this is typical for FDSs. Thus, we can neglect the boundary layer and consider a fully developed periodic FDS solution $u_{\text{FDS}}(x + P) = u_{\text{FDS}}(x)$ and $v_{\text{FDS}}(x + P) = v_{\text{FDS}}(x)$, where P is the period. To analyze the stability of this solution we introduce a small perturbation, $u = u_{\text{FDS}}(x) + U(x)e^{-i\omega t}$ and $v = v_{\text{FDS}}(x) + V(x)e^{-i\omega t}$, where the frequency ω plays a role of an additional parameter. ω is real because the perturbation appears due to an external forcing that has a stationary amplitude. After the substitution into Eqs. (1), for small $U(x)$ and $V(x)$ we obtain the following linear equations with periodic coefficients:

$$U'' - \phi U' = (1 - i\omega + 4F_1(x))U + 4F_2(x)V, \quad (8a)$$

$$\delta V'' - r\phi V' = b(F_1(x) - 1)U - (i\omega - bF_2(x))V, \quad (8b)$$

where $F_1 = v_{\text{FDS}}(1 - u_{\text{FDS}}^2)/(1 + u_{\text{FDS}}^2)^2$ and $F_2 = u_{\text{FDS}}/(1 + u_{\text{FDS}}^2)$. These second order equations have complex coefficients. After straightforward transformations they can be re-written as eight real equations of the first order.

Similar approach in a context of FDO/FDS patterns was developed by McGraw and Menzinger [8] who studied small perturbations to the steady state and considered linear modes having real frequencies. This type of modes corresponds to a stationary forcing at the inlet. The essential difference of our study is the consideration of small perturbations to a *fully developed* FDS pattern. The linearized equations (8) in this case have periodic coefficients and we should apply the Floquet theorem to analyze its stability properties.

As follows from the Floquet theorem [35] the system has eight eigensolutions $\vec{v}(x)$ and eight corresponding eigenvalues λ for which

$$\vec{v}(x + P) = \lambda \vec{v}(x). \quad (9)$$

There are four couples of λ , either real and identical or complex conjugated. Their absolute values can be labelled as $|\lambda|_1 \leq |\lambda|_2 \leq |\lambda|_3 \leq |\lambda|_4$. These values

depend on the parameters of the system and on the forcing frequency ω . For $\phi > \phi_{\text{FDS}}$ the two highest values always correspond to diverging solutions of Eqs (8), $|\lambda|_3 > 1$ and $|\lambda|_4 > 1$, while the others always represents a stable solution, $|\lambda|_1 < 1$. The stability of FDS is characterized by $|\lambda|_2$. FDS is stable if $|\lambda|_2 < 1$ for any ω while it is unstable when $|\lambda|_2 > 1$ for certain values of ω . It is more convenient to consider a characteristic exponent that does not depend on the period of FDS,

$$\rho_i = (\ln |\lambda|_i)/P. \quad (10)$$

So, in a critical point of the linear stabilization the global maximum of $\rho_2(\omega)$ passes zero.

We compute the eigenvalue $|\lambda|_2$ using the Floquet theorem. The idea of this approach can be found, for example, in [35]. Let \hat{A} be a linear evolution operator advancing a solution over the period, $\hat{A}\vec{v}(x) = \vec{v}(x + P)$. Each eigenvector \vec{v} can be decomposed over the unit basis as $\vec{v} = \sum_{i=1}^8 \vec{e}_i c_i$, where \vec{e}_i are the unit vectors and c_i are the coefficients of the decomposition. Taking this into account, we obtain from Eq. (9):

$$\sum_{i=1}^8 (c_i \hat{A} \vec{e}_i) = \lambda \sum_{i=1}^8 (c_i \vec{e}_i). \quad (11)$$

These equations have a nontrivial solution for the coefficients c_i if λ is an eigenvalue of the matrix with columns $\hat{A}\vec{e}_i$. To obtain this matrix, we find numerically a noiseless FDS solution and extract a full period. Then, we interpolate it with polynomials and substitute the resulting functions into Eqs. (8). Starting from the unit vectors \vec{e}_i ($i = 1 \dots 8$), we find eight solutions to these equations over the period and obtain the sought matrix. Finally, we compute the eigenvalues and, after sorting by their absolute values, take the second one.

A numerical analysis shows that on the FDS onset $\phi = \phi_{\text{FDS}}$ the number of maxima of $\rho_2(\omega)$ coincides with the number of linear modes, stable or unstable, of Eqs. (1). There is at least one couple of symmetric maxima corresponding to Hopf or DIFI modes that are responsible for the formation of FDS. Without a differential flow, the system can also display a Turing mode. In this case $\rho_2(\omega)$ acquires another couple of maxima. For example in Fig. 11 the first maxima from the origin correspond to the Hopf mode and the second pair correspond to the Turing mode. All the maxima are positive, hence the FDS is unstable.

The system (8) can be considered as a linear amplifier of an inlet forcing where $\rho_2(\omega)$ is an amplification ratio. As follows from Fig. 11 the amplification is selective. When a wide-band noise passes thorough the system, noise harmonics grow if corresponding $\rho_2(\omega)$ is positive. All other harmonics decay. As a result, oscillations at the outlet consist of harmonics that are gathered around

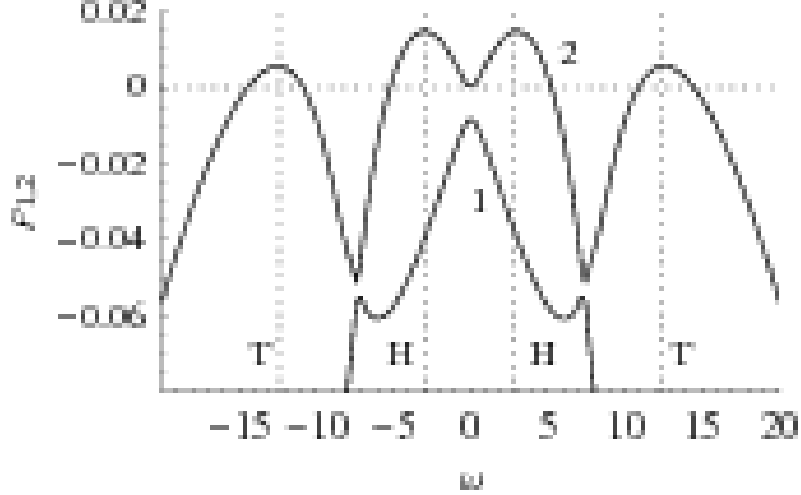


Figure 11. Characteristic exponents ρ_1 and ρ_2 vs. ω . Curve $\rho_2(\omega)$ has two positive maxima indicating the instability of corresponding FDS. Positions of the maxima coincide with the frequencies of Hopf and Turing modes that are indicated by the dashed lines “H” and “T”, respectively. $a = 15$, $b = 5.5$, $\delta = 10$, $r = 1$, $\phi = 13$.

maxima of $\rho_2(\omega)$, i.e. around linear modes of the initial system (1). This is remarkably coincides with our qualitative observations in the above sections: when an FDS is unstable inlet noise stimulates the growth of an unstable linear mode to an oscillatory solution.

When the flow rate grows the structure of $\rho_2(\omega)$ varies in two different ways. The first one is illustrated in Fig. 12. This corresponds to the first scenario of the FDS stabilization that is represented in Fig. 10(a,b and c) and has been discussed in Sec. 4. Different curves in Fig. 12 are plotted for different flow rates:

- (1) The curve ρ_2 has two positive maxima. Selected noise harmonics excites oscillatory mode which destroy the FDS. Hence the is linearly unstable.
- (2) The first maximum moves towards the origin while the second one becomes negative. The Turing mode can not be excited any more, but the other one (i.e., the Hopf mode in this figure, but also it can be a DIFI mode) destroys the pattern. The system is still unstable.
- (3) The first maximum continues the moving to origin. Thus, frequencies of selected noise harmonics differ more and more from the Hopf frequency. Because of this detuning the excitation of Hopf oscillations becomes less effective.
- (4) Two symmetric maxima (the left one is not shown) merge with a central minimum and these three extremums transform into a single maximum at the origin. Now all the noise harmonics have non-positive amplification ratio and those which are close to the Hopf mode are even suppressed. As a result, the noise can not excite oscillations. The FDS is linearly stable.

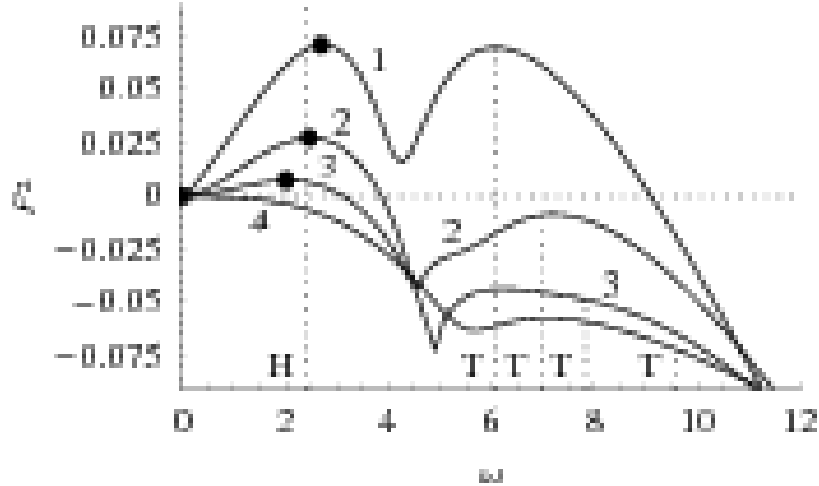


Figure 12. First scenario of the FDS stabilization. Bullet points show the successive positions of the right maximum (the left symmetric maximum is not shown) as the flow rate grows. Line “H” indicates the Hopf frequency and “T” mark the Turing frequencies for different flow rates. $a = 15$, $b = 4$, $\delta = 10$, $r = 1$, $\phi_1 = 7$, $\phi_2 = 8$, $\phi_3 = 9$, $\phi_4 = 11$.

Because the second couple of maxima passes zero first, it does not play an important role in the stabilization. Thus, we classify as the first scenario all cases when these maxima absent at all. For example, these cases are shown in Fig. 10(a,b).

Fig. 13 corresponds to the second scenario that has been shown in Fig. 10(d):

- (1) There are two positive maxima and the FDS is linearly unstable.
- (2) The first maxima merge (only the right part of the symmetric curve is shown) but the second ones are still positive and thus responsible for the instability of FDS.
- (3) The second couple of maxima pass zero (only the right one is shown in the figure). As a result, no oscillations are excited and the FDS becomes stable.

So we see that two scenarios of the FDS stabilization that have been revealed from numerical simulations now are confirmed by a linear stability analysis.

We can provide a direct verification of linear nature of the instability of FDS near the critical point ϕ_{FDS} . Let us suppose that the inlet perturbation is nearly equal to the saturated FDS amplitude, so that we can neglect the boundary layer of an FDS pattern. In the presence of inlet noise with an amplitude θ , the FDS occupies an area of a finite size, say h . At the right edge of this area the noise reaches the amplitude θ_1 which is sufficient to destroy the FDS. If the instability is linear, we can write $\theta_1 = \theta e^{h\rho_2}$, where $\rho_2 \equiv \rho_2(\omega_{\text{max}})$ is the characteristic exponent responsible for the stability of FDS. Hence, the size of

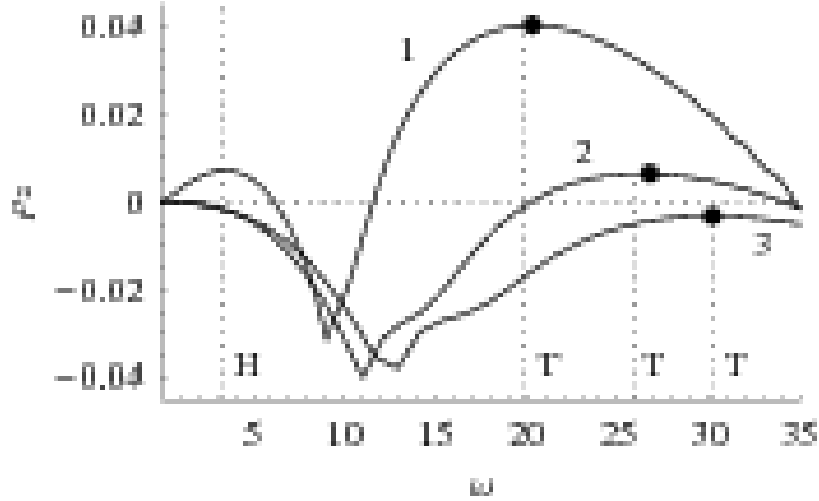


Figure 13. Second scenario of the linear stabilization of FDS. Bullet points show how the second maximum becomes negative as the flow rate grows. $a = 20$, $b = 9$, $\delta = 20$, $r = 1$, $\phi_1 = 23$, $\phi_2 = 30$, $\phi_3 = 35$.

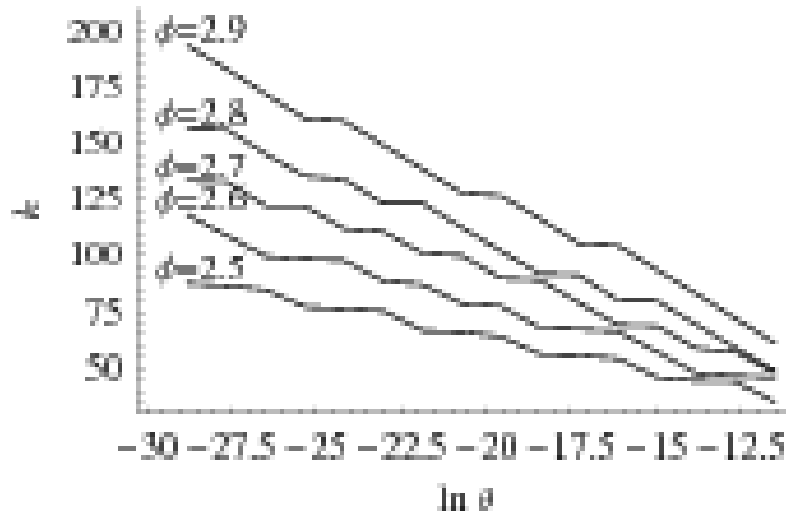


Figure 14. Size of an area of a localized FDS h vs. logarithm of the noise amplitude θ . Observe linear dependance as predicts Eq. (12) $a = 20$, $b = 3.5$, $\delta = 3$, $r = 1$.

an FDS area varies linearly with the logarithm of the noise amplitude as

$$h = (\ln \theta_1 - \ln \theta) / \rho_2. \quad (12)$$

This equation can easily be verified directly. Solving numerically Eqs. (1) for different noise amplitudes, we can find corresponding sizes of the FDS area. Fig. 14 displays the resulting curves obtained for different flow rates. As expected, h decays linearly with $\ln \theta$.

Eq. (12) can be used for experimental measuring of the critical flow rate of linear stabilization ϕ_0 . A factor in Eq. (12) is the reciprocal characteristic ex-

ponent $\rho_2(\omega_{\max})$. To find this factor one needs to vary amplitude of the inlet fluctuations and measure the size h of the FDS area. Unfortunately, it is not easy to perform this practically. But because we deal with a linear problem, each inlet harmonic is amplified separately. So we can substitute the fluctuations with the most amplified harmonic¹. The size h of the corresponding FDS area should be equal to that producing by a wide-band inlet noise. The frequency of this harmonic is ω_{\max} . This value may be calculated using the Floquet theorem as we have done above for our system. Thus varying the amplitude θ of the inlet forcing and measuring corresponding sizes h one can obtain a line $h(\ln \theta)$ and then calculate ρ_2 as an inverse slope of this line. After that one needs to repeat the measuring at different flow rates. Knowing ρ_2 vs. flow rate, one can extrapolate the dependance $\rho_2(\phi)$ to a point where ρ_2 vanishes and find the critical flow rate ϕ_0 .

6 Summary and results

We studied the stability of FDS patterns in presence of a noise at the inlet. The following picture was revealed. If the flow rate is not so high, fluctuations at the inlet stimulate the growth of an oscillatory mode and thus prevents the formation of FDS. For higher flow rates, however, an FDS pattern becomes linearly stable. We found two scenarios of the linear stabilization: 1) detuning of the most amplified noise harmonics from the resonance with an oscillatory mode; 2) stopping of a noise amplification.

In our previous paper [26] we showed that linearly stable FDS pattern still can be destructed by a noise if its amplitude is sufficiently high. A threshold value of the noise amplitude depends on the flow rate as a power law. Or vice versa: for a fixed noise amplitude there is a flow rate above which an FDS pattern becomes stable. This was referred to as a nonlinear instability of FDS. In present paper we consider all possible FDSs: 1) FDS is a stationary spatial distribution of Hopf oscillations; 2) FDS emerges because of presence a DIFI; 3) FDS based on the Hopf mode appears when also a Turing mode is present and both Hopf and Turing modes have high growth rates; 4) FDS appears when the Turing mode is much stronger then the Hopf mode. These numerical experiments confirm our previous analysis. Also, the numerical simulations reveal two scenarios of the stabilization that remarkably correspond to those found within a linear approach.

Let us consider an equation for a perturbation to FDS. (Now we mean the

¹ Experiments where FDS is forced by a periodic oscillations at the inlet are reported by Kærn and Menzinger [4,5] and also similar problem is considered by Taylor at al. [17].

nonlinear equation whose linearized version has been studied in Sec. 5, see Eq. (8).) Our observations can be summarized in terms of bifurcations of the perturbation equation. A qualitative picture is following. When an FDS is linearly unstable, the perturbation equation has a kind of unstable fixed point. A bifurcation takes place when the flow rate grows and our analysis predicts two scenarios for this. The result of the bifurcation is the split of the unstable fixed point into a stable fixed point and unstable limit cycle. This corresponds to a nonlinear instability of the FDS. Small inlet noise decays because the system remains close to the stable fixed point. But higher noise brings out the system above the unstable limit cycle. An amplification of noise results in the destruction of FDS. If we increase the flow rate while keeping the noise amplitude unaltered, a position of the limit cycle changes and the system returns back to a vicinity of the stable fixed point. The unstable limit cycle inherits properties of the unstable fixed point, so that two scenarios of stabilization are observed when the system passes this cycle. These are the scenarios that are obtained in numerical experiments in Secs. 3 and 4.

The destruction of FDS in presence of an inlet noise takes place because this periodic pattern serves as a selective amplifier of the forcing. The highest amplification takes place at frequency equal to an unstable oscillatory mode. This resonant interaction excites the oscillatory solution that suppresses the FDS. Hence, the specific type of an inlet forcing is not very important. The sufficient requirement is that its spectrum contain harmonics close to the resonance. In particular, it means that our results remain valid for a Gaussian noise. We tried this type of noise. The results were qualitatively similar.

A pure periodic forcing at the inlet is already studied well. As reported in [4,5,17], the inlet oscillations of concentrations stimulate the destruction of FDS provided that the frequency is close to the natural frequency of a system. In other words, the destruction takes place when the forcing is in the resonance with a mode responsible for the formation of FDS. A minor decreasing of the inlet frequency from the resonance results in the pulsating waves as in [4] or in the zigzag patterns [17]. These structures are very similar to our intermediate situations represented in Figs. 2(b) and 7(b). These results, in fact, correspond to our first scenario of the FDS stabilization via detuning from the resonance.

Also the resonance with the natural frequency of a system is reported by McGraw and Menzinger [15]. They apply a periodic modulation to the flow rate and observe a localized FDS area suppressed downstream by an oscillatory solution. It is interesting that the suppression takes place not only at the natural frequency. The resonance and further suppression is also observed at nonlinear ratios 2 : 1 and 3 : 1!

Finally, we suggest an idea for an experimental measuring of a flow rate of

linear stabilization. Applying to the FDS inlet a weak periodic forcing with specific frequency one can find a characteristic exponent that is responsible for the linear instability. One needs to find this exponent for different flow rates and then extrapolate the dependance to a point where the exponent vanishes. A corresponding flow rate is the sought critical value of the linear stabilization.

This work was partially supported by grant of RFBR (no. 04-02-04011).

References

- [1] S. P. Kuznetsov, E. Mosekilde, G. Dewel, P. Borckmans, Absolute and convective instabilities in a one-dimensional Brusselator flow model, *J. Chem. Phys.* 106 (1997) 7609–7616.
- [2] P. Andresén, M. Bache, E. Mosekilde, G. Dewel, P. Borckmans, Stationary space periodic structures with equal diffusion coefficients, *Phys. Rev. E* 60 (1999) 297–301.
- [3] M. Kærn, M. Menzinger, Flow-distributed oscillations: Stationary chemical waves in a reacting flow, *Phys. Rev. E* 60 (1999) R3471–R3474.
- [4] M. Kærn, M. Menzinger, Pulsating wave propagation in reactive flows: Flow-distributed oscillations, *Phys. Rev. E* 61 (2000) 3334–3338.
- [5] M. Kærn, M. Menzinger, Experiments on flow-distributed oscillations in the Belousov–Zhabotinsky reaction, *J. Phys. Chem. A* 106 (19) (2002) 4897–4903.
- [6] R. A. Satnoianu, P. K. Maini, M. Menzinger, Parameter space analysis, pattern sensitivity and model comparison for Turing and stationary flow-distributed waves (FDS), *Physica D* 160 (2001) 79–102.
- [7] R. A. Satnoianu, Coexistence of stationary and traveling waves in reaction–diffusion–advection systems, *Phys. Rev. E* 68 (2003) 032101.
- [8] P. N. McGraw, M. Menzinger, Pattern formation by boundary forcing in convectively unstable, oscillatory media with and without differential transport, *Phys. Rev. E* 72 (2005) 026210.
- [9] R. A. Satnoianu, M. Menzinger, Non-Turing stationary patterns in flow-distributed oscillators with general diffusion and flow rates, *Phys. Rev. E* 62 (2000) 113–119.
- [10] P. V. Kuptsov, Rigid transition to the stationary structure and imposed convective instability in a reaction–diffusion system with flow, *Physica D* 197 (2004) 174–195.
- [11] D. G. Míguez, R. A. Satnoianu, A. P. Muñuzuri, Experimental steady pattern formation in reaction-diffusion-advection systems, *Phys. Rev. E* 73 (2) (2006) 025201.

- [12] D. G. Míguez, G. G. Izús, A. P. Muñuzuri, Robustness and stability of flow-and-diffusion structures, *Phys. Rev. E* 73 (1) (2006) 016207.
- [13] P. V. Kuptsov, S. P. Kuznetsov, E. Mosekilde, Particle in the brusselator model with flow, *Physica D* 163 (2002) 80–88.
- [14] J. R. Bamforth, R. Toth, V. Gaspar, S. K. Scott, Scaling and dynamics of “flow distributed oscillation patterns” in the Belousov–Zhabotinsky reaction, *PCCP* 4 (8) (2002) 1299–1306.
- [15] P. N. McGraw, M. Menzinger, Flow-distributed oscillation, flow-velocity modulation, and resonance, *Phys. Rev. E* 72 (2005) 027202.
- [16] P. V. Kuptsov, R. A. Satnoianu, P. G. Daniels, Pattern formation in 2D reaction–diffusion channel with Poiseuille flow, *Phys. Rev. E* 72 (2005) 036216.
- [17] A. F. Taylor, J. R. Bamforth, P. Bardsley, Complex pattern development in a plug-flow reactor, *PCCP* 4 (22) (2002) 5640–5643.
- [18] W. van Saarloos, Front propagation into unstable states: Marginal stability as a dynamical mechanism for velocity selection, *Phys. Rev. A* 37 (1988) 211–229.
- [19] W. van Saarloos, Front propagation into unstable states. II. Linear versus nonlinear marginal stability and rate of convergence, *Phys. Rev. A* 39 (1989) 6367–6390.
- [20] P. V. Kuptsov, S. P. Kuznetsov, C. Knudsen, E. Mosekilde, Absolute and convective instabilities in the one-dimensional Brusselator model with flow, *Recent Res. Devel. Chem. Physics* 4 (2003) 633–658.
- [21] R. J. Deissler, Noise-sustained structure, intermittency, and the ginzburglandau equation, *J. Stat. Phys.* 40 (1985) 371–395.
- [22] R. J. Deissler, J. D. Farmer, Deterministic noise amplifiers, *Physica D* 55 (1992) 155–165.
- [23] P. Borckmans, G. Dewel, A. D. Witt, D. Walgraef, The differential flow instabilities, in: K. S. R. Kapral (Ed.), *Chemical Waves and Patterns*, Kluwer Academic Publishers, Dordrecht, 1995, pp. 87–95.
- [24] P. S. Landa, Turbulence in nonclosed fluid flows as a noise-induced phase transition, *Europhys. Lett.* 36 (6) (1996) 401–406.
- [25] S. P. Kuznetsov, Noise-induced absolute instability, *Mathematics and Computers in Simulation* 58 (2002) 435–442.
- [26] P. V. Kuptsov, R. A. Satnoianu, Stability of Flow– and Diffusion Distributed Structures (FDS) to inlet noise effects, *Phys. Rev. E* 71 (2005) 015204.
- [27] I. Lengyel, I. Epstein, Modelling of Turing structures in the chlorite–iodide–malonic acid–starch reaction system, *Science* 251 (1991) 650–652.
- [28] O. Jensen, V. O. Pannbacker, E. Mosekilde, G. Dewel, P. Borckmans, Localized structures and front propagation in the Lengyel–Epstein model, *Phys. Rev. E* 50 (2) (1994) 736–749.

- [29] A. M. Turing, The chemical basis of morphogenesis, *Philos. Trans. R. Soc. B* 237 (1952) 37–72.
- [30] G. Nicolis, I. Prigogine, *Self-Organization in Nonequilibrium Systems*, Wiley, New York, 1977.
- [31] M. Kærn, M. Menzinger, R. A. Satnoianu, A. Hunding, Chemical waves in open flows of active media: Their relevance to axial segmentation in biology, *J. R. Chem. Soc., Faraday Discussions* 120 (2002) 295–312.
- [32] A. B. Rovinsky, M. Menzinger, Self-organization induced by the differential-flow of activator and inhibitor, *Phys. Rev. Lett.* 70 (1993) 778–781.
- [33] P. Andresén, E. Mosekilde, G. Dewel, P. Borckmans, Comment on “Flow-distributed oscillations: Stationary chemical waves in a reacting flow”, *Phys. Rev. E* 62 (2) (2000) 2992–2993.
- [34] M. Kærn, M. Menzinger, Reply to “Comment on ‘Flow-distributed oscillations: Stationary chemical waves in a reacting flow’ ”, *Phys. Rev. E* 62 (2) (2000) 2994–2995.
- [35] D. W. Jordan, P. S. Smith, *Nonlinear ordinary differential equations*, Clarendon press, Oxford, 1987.